Novel Phase Shifter Based on Dielectric Resonator on Liquid Crystal Substrate

S. A. Attya [1], Nihal F. F. Areed [1,2], Mohamed Farhat O. Hameed [2], M. A. El-Razzak [1], and Salah Sabry A. Obayya [2]

[1] Department of Electronics and Communications Engineering
Faculty of Engineering, Mansoura University, Mansoura 35516, Egypt
seham_abdo@mans.edu.eg, nahoolaf@yahoo.com, mabdelrazzak@hotmail.com

[2] Center for Photonics and Smart Materials
Zewail City of Science and Technology, Sheikh Zayed District, 6th of October City, 12566, Egypt
nfayez@zewailcity.edu.eg, mfarahat@zewailcity.edu.eg, sobayya@zewailcity.edu.eg

Abstract ― In this paper, a novel design of microwave phase shifter with enhanced high level of flexible integration is proposed and analyzed using 3D finite difference time domain. The proposed design is based on the combination of dielectric resonators and nematic liquid crystal (NLC) layer of type E7. The effects of the structure geometrical parameters on the transmission angle are carried out. Based on the simulation results, optimizations of the geometries are curial for varying the phase of the transmitted signal. In addition, the use of NLC layers placed in silica pan as a substrate to the dielectric resonator offers a number of advantages over existing microwave phase shifters such as simple design, high bandwidth and phase tunability. Moreover, the suggested design has an excellent potential for being very useful in microwave encryption systems.

Index Term ― Dielectric resonator filter, finite difference time domain, liquid crystal, phase shifter.

I. INTRODUCTION

Dielectric resonator (DR) has primarily been used in microwave circuits, such as oscillators [1], filters [2], and recently as antenna [3]. The DR is normally made of high-permittivity material, with dielectric constant $\varepsilon_r > 20$. The unloaded Q-factor of the DR can be as high as 10,000 [4]. In addition, inexpensiveness, high power tolerance and high temperature stability can be achieved [5].

The DR structures are divided into two basic configurations: individual dielectric resonators that are loaded axially in metal enclosures, in which it is difficult to physically support the resonators [6-8], or individual resonators that are mounted in a planar configuration [9-12]. In the latter case, DRs are centered in position and mounted inside a filter housing using a support of low-dielectric-constant and low-loss material.

Phase shifters are one of the key elements for future reconfigurable radio frequencies (RF) devices. Widely known technologies include passive tunable dielectrics like barium-strontium-titanate (BST) [13], micro-electro-mechanical system (MEMS) [14] and semiconductor solutions are mostly based on varactor diodes [15]. Also, liquid crystal (LC) can give very promising opportunity to realize tunable RF devices. The LC material consists of anisotropic molecules, where by applying an external electrical field, the molecules of the LC type start to align along the field lines. The magnitude of the orientation is depending on the field strength. Due to the anisotropy of the molecules, this effect can be employed to tune the effective permittivity of the LC layer inside the device continuously [16].

This work represents new numerical finite difference time domain (FDTD) calculations of the transmission angle of the DR bandpass filter proposed by [17]. Simulation effects of the geometrical parameters on the transmission angle

Submitted On: March 25, 2014
Accepted On: January 3, 2015

are carried out. Based on the simulation results, optimizations of the geometries are crucial for varying the phase of the transmitted signal. A simple implementation of tunable phase shifter is proposed and based on inserting a thin layer of liquid crystal material of type E7 as a substrate in the considered DR structure. By this way, an electrical frequency dependent tunable phase shifter can be obtained. Furthermore, this work has opened up an entirely new direction for the usage of the presented phase shifter as a real time encryptor in various communication systems.

II. DEVICE ARCHITECTURE

Figures 1 (a) and 1 (b) show 3-D view and front view of the conventional DR [17], respectively. As shown from the figure, the DR structure consists of two cylindrical dielectric discs made of ceramic type material ($Ca_5Ta_2Tio_{12}$) of ε_r =38 separated by a distance ζ. The two dielectric discs of radius R, and relative permittivity ε_r act as coupled resonators such that the entire device becomes high quality bandpass filter which feed through two coaxial coupler. One of the coaxial coupler is used as an input port while the other is taken as the output port. These two ports are drilled on a metallic ground plane substrate of thickness h. The two dielectric discs are placed above the ground plane with an offset distance d (air substrate height).

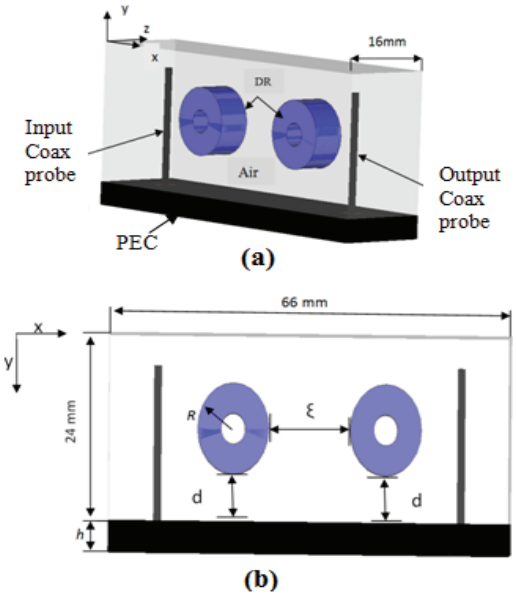

Fig. 1. DR geometry details: (a) 3D view, (b) front view.

III. SIMULATION RESULTS

Firstly, 3D FDTD method is used to investigate the effects of the mesh size on the accuracy of the simulation results. In this study, the DR geometrical parameters are taken as d= 6 *mm*, R = 5.85 mm, and ζ = 13.5 mm, h = 3.9 mm, ε_r = 38. In addition, the substrate has dimensions of 66×16 mm and the surrounding space has dimensions of 66×24×16 mm. Figure 2 (a) shows the variation of S_{21} parameter with different mesh densities. It can be noted from this figure that to keep a reasonable accuracy, this structure should be discretized with a mesh cell size equal to λ/35 or less. Figure 2 (b) shows variation of magnitude of S_{21} and frequency calculated by finite integration time domain (FITD) [17], and that obtained by FDTD [18-20] at different mesh densities. It is evident from the figure that there is a good agreement between the presented results and the published results by [17] where, the operating resonant frequency for the considered bandpass filter is equal to 4.525 GHz.

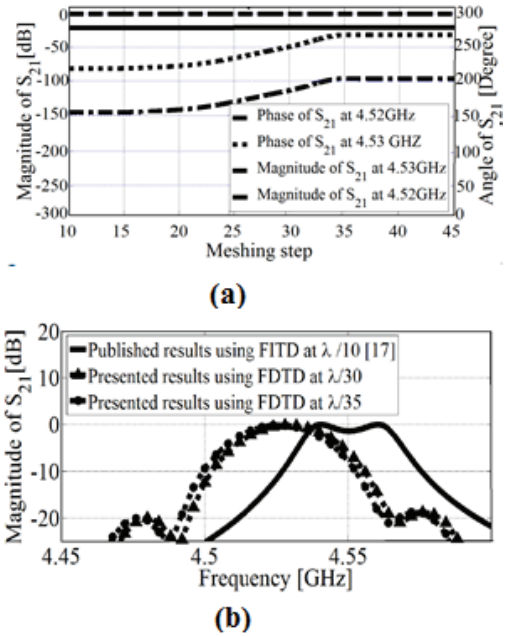

Fig. 2. Simulation of DR: (a) transmission coefficients vs. meshing step, (b) magnitude of S_{21} vs. frequency.

The effect of the structure geometrical parameters that may affect the angle of the transmission signal to the output coaxial port is investigated. In this study, the initial parameters are

chosen to be h = 3.9 mm, R = 5.85 mm, d = 6 mm, and ζ = 13.5 mm. It should be noted that, the numerical simulations reveal that to maintain bandpass performance, the ranges of h, R, d, and ζ are chosen to be (1:11), (5.85:5.87), (4:8), (10:17) in mm, respectively.

First, the effect of the ground plane thickness (h) on the transmission angle is studied while the other parameters d, R, and ζ are kept constant at their initial values. Figure 3 (a) shows the calculated S_{21} angle for different values of the ground plane thickness (h) at two different frequencies, 4.52 GHz and 4.53 GHz. It can be noted from this figure that the phase of S_{21} (θ) decreases linearly as ground plane thickness increases and this linear relation can be equated as follows:

$$\Theta = -Ah+B, \quad (1)$$

where the calculated value of A is around 16.87 and the value of B is variable that depends on the resonant frequency. The correlation coefficient $r^2 \approx 1$ between the fitting data and the original data indicates that a linear approximation is a good fit to this data. The small variability in the data and the large number of data points have resulted in a small standard deviation of 5×10^{-4} between an angle-estimate for a given value of h. It should be noted that, any positive or negative output phase can be easily obtained by changing the ground plane thickness. For example, at the operating frequency 4.52 GHz, the phase +90º and the complementary phase -90º can be easily obtained by using ground planes of thickness 1 mm and 11 mm, respectively. These obtained phase values can be used in encryption.

Next, the effect of the outer radius (R) of the dielectric disc on the transmission angle is studied while the other parameters d, h, and ζ are kept constant at 6 mm, 3.9 mm, and 13.5 mm, respectively. Figure 3 (b) shows the calculated angle of S_{21} as a function of R at two different frequencies 4.52 GHz and 4.53 GHz. It is evident from the figure that, the phase of S_{21} decreases with increasing the outer radius of the dielectric disc, and this linear relation is estimated as follows:

$$\Theta = -AR+B, \quad (2)$$

where the calculated value of A is around 3465.8 and the value B is a variable that depends on the resonant frequency. The correlation coefficient $r^2 = 0.9988$ between the fitting data and the original data indicates that a linear approximation is a good fit to this data. The large variability in the data and the large number of data points have achieved a small standard deviation of 0.6868 between an angle-estimate for a given value of R.

It should be noted from Fig. 3 (b), that at the operating frequency 4.52 GHz, the phase +90º can be easily obtained by setting the outer radii of the two dielectric discs to 5.855 mm.

The effect of air substrate height (d) on the transmission angle is also investigated while the other parameters R, h, and ζ are kept constant at 5.85 mm, 3.9 mm, and 13.5 mm, respectively. The correlation coefficient r^2 = 0.9 between the fitting data and the original data indicates that a parabolic approximation is a good fit to this data. The small variability in the data and the large number of data points have resulted in a small standard deviation of 0.14597 between an angle-estimate for a given value of d. Figure 3 (c) shows the calculated angle of S_{21} for different values of air substrate height (d) at two different frequencies, 4.52 GHz and 4.53 GHz. It can be found form the figure that, the relation between them follows a parabolic shape where the phase decreases by increasing the offset distance d from 4 to 6 mm, while the phase increases with increasing offset distance from 6 to 8 mm.

The effect of the separation distance between the two dielectric discs (ζ) on the transmission angle is also studied while the other parameters R, h, and d are kept constant. Figure 3 (d) shows the numerical analysis of S_{21} for different values of (ζ) at two different frequencies, 4.52 GHz and 4.53 GHz. It is evident from this figure that, the phase values of S_{21} tend to be constant with increasing the value of ζ. The correlation coefficient r^2 = 0.994 between the fitting data and the original data indicates that a parabolic approximation is a good fit to this data. The small variability in the data and the large number of data points have produced in a small standard deviation of 0.133925 between an angle-estimate for a given value of ζ.

Based on the above geometrical study, -90º

phase shifters at the operating frequency 4.52 GHz with allowable bandwidth of 1 MHz can be obtained using the considered structure shown in Fig. 1 with R = 5.87 mm while the other parameters d, h and ζ are taken as 6 mm, 10.9 mm and 13.5 mm, respectively. Further, +90° phase shift can be obtained at R to be 5.8525 mm, as shown in Fig. 4 (a). Also, physical movement of the dielectric discs above the ground plane results in tunable phase shifter with allowable range -21° to 21° at the operating frequency 4.53 GHz when dielectric disc is moved above the ground plane with dielectric discs radius of 5.87 mm, as shown in Fig. 4 (b).

Figures 4 (c) and 4 (d) show the steady state z-polarized magnetic field distributions along the *xy*-plane at frequencies of 4 GHz and 4.53 GHz, respectively. It is evident from these figures that, the field along the structure is highly confined at port 1 at f = 4 GHz, while at f = 4.53 GHz the field propagates from port 1 to port 2. These field distributions confirm the behavior of S_{21} shown earlier in Figs. 4 (a) and 4 (b). Figure 4 (e) demonstrates the steady state distributions of the *z*-polarized magnetic field along the propagation x direction at the wavelength of 10.7 mm for the chosen ground plane thicknesses h = 0.9 mm and 10.9 mm, respectively. It can be observed from the figure that, the transmitted signal at h = 10.9 mm overrides the transmitted signal at h = 0.9 mm by about $\ell = \lambda/2$, which clearly fits with the behavior of the argument of S_{21} shown in Fig. 4 (a).

The designed phase shifter has some limitation such as complexity of design, implementation and physical movement which is obtained using an electrically driven actuator. The actual configuration can vary considerably from 'trombone' transmission lines adjusted by stepper motor to dielectric/capacitive loading adjusted with solenoid/piezo-electric actuators. The most common is the 'trombone' type and these are usually associated with high-precision bench top test equipment, rather than high volume use [21].

By using values in Fig. 4 (a), the proposed phase shifter can be used as asymmetric hardware key for data encryption and decryption as referenced by Nihal, *et al*. [22]. The phase of the audio data can be encoded by adding a constant phase shift 90° within the frequency band of the signal. However, complementary phase shift -90° will be added to decode the signal. The accuracy of retrieved signal is estimated through root mean squared error (RMS) calculations which equals to 3.6333×10^{-4}.

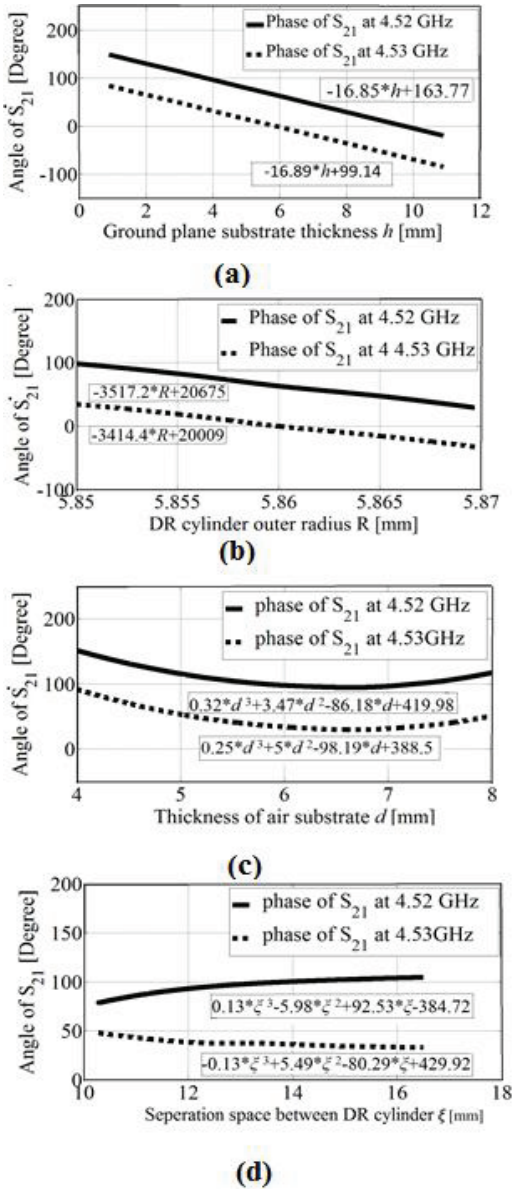

Fig. 3. Effect of geometrical parameters on the phase of S_{21}: (a) ground plane thickness, (b) dielectric disc outer radius, (c) thickness of air substrate, and (d) separation between two dielectric discs.

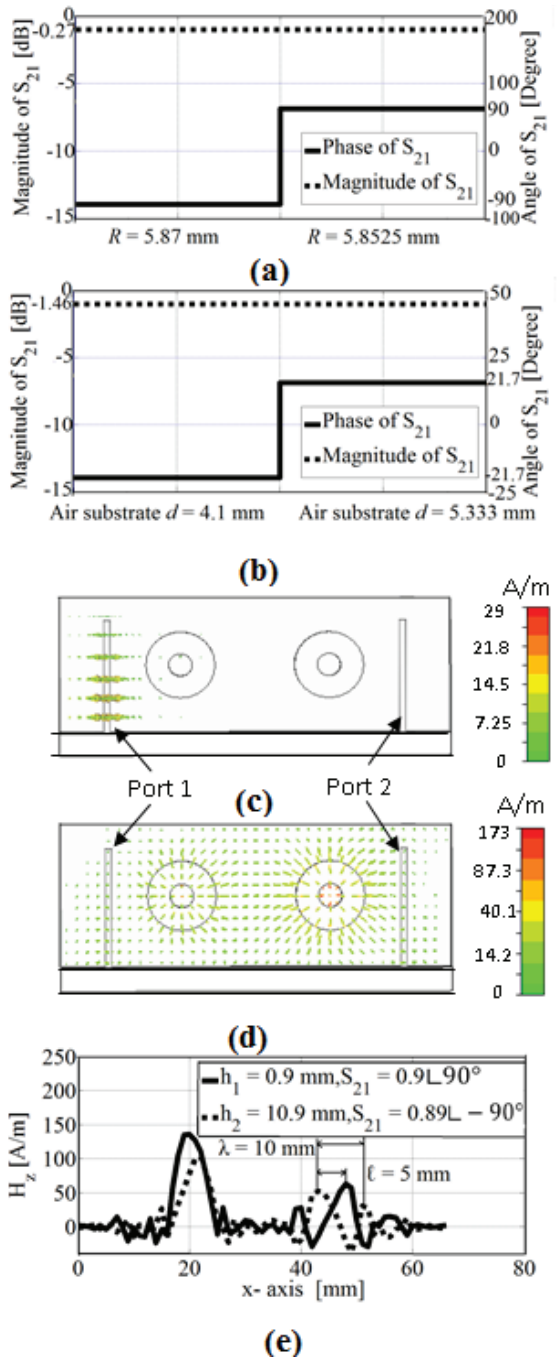

Fig. 4. (a) Simulated S_{21} at 4.52 GHz, (b) simulated S_{21} at 4.53 GHz, (c) 2D z-magnetic field along *xy*-plane at 4 GHz, (d) 2D z-magnetic field along *xy*-plane at 4.53 GHz, and (e) 1D z-magnetic field along *x-axis* at y = -10.3 mm and z = 8 mm.

It is observed from the analysis that the designed phase shifter has some limitation such as mechanical variations. In this study, liquid crystals layer can be used as a substrate to the considered dielectric resonator instead of air to obtain an electrical tunable phase shifter as shown in Fig. 5. The LC consists of anisotropic molecules. The rod-shaped molecules tend to align themselves along the surface. When applying an external electrical field, the molecules of the LC start to align along the field lines. The magnitude of the orientation is depending on the field strength. Due to the anisotropy of the molecules, this effect can be employed to tune the effective permittivity of the LC layer inside the device continuously [16,22-24]. The LC has two principal refractive indices, ordinary refractive index n_o and extraordinary refractive index n_e. The first one, n_o, is measured for the light wave where the electric vector vibrates perpendicular to the optical axis (ordinary wave). However, the index n_e is measured for the light wave where the electric vector vibrates along the optical axis (extraordinary wave). Then the birefringence (Δn) is given by:

$$\Delta n = n_e - n_o. \quad (3)$$

The nematic liquid crystal (NLC) used in the proposed structure is of type E7 with relative permittivity tensor $\underline{\varepsilon_r}$ [22-24]:

$$\varepsilon_r = \begin{pmatrix} n_o^2 \sin^2\varphi + n_e^2 \cos^2\varphi & (n_e^2 - n_o^2)\cos\varphi\sin\varphi & 0 \\ (n_e^2 - n_o^2)\cos\varphi\sin\varphi & n_o^2\cos^2\varphi + n_e^2\sin^2\varphi & 0 \\ 0 & 0 & n_o^2 \end{pmatrix}, \quad (4)$$

where φ is the molecule rotation angle.

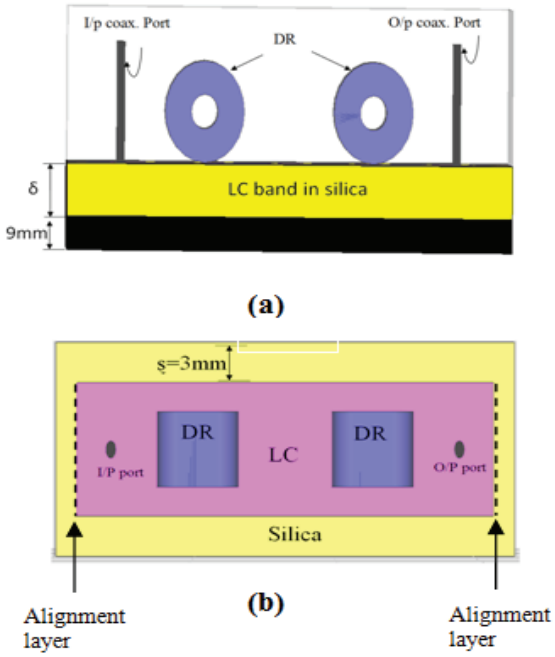

Fig. 5. Electrical tunable phase shifter structure: (a) front view, (b) top view.

Glass cavity filled with LC of type E7 is used as a substrate for the considered dielectric resonator. Two alignment layers along the *x*-axis have to be used to align the molecules along the y-axis (unbiased state), as shown in Fig. 5.

The effect of varying the thickness of the unbiased liquid crystal (δ) on the phase of the transmitted wave has been studied as shown in Fig. 6 (a). As shown in this figure, liquid crystal thickness below 3 mm results in bandstop filter. If the thickness is further increased beyond 3 mm, bandpass filter will be obtained. By changing the biasing state of the LC, the applied voltage across the biasing layers along the *x*-axis rotates the LC molecules. At saturation the director is oriented perpendicular to the cell wall along *x*-axis, with rotation angle $\varphi = 90^o$. It should be noted that changing the biasing voltage will vary the phase of the transmitted signal. Hence, using liquid crystal with thickness 8 mm and changing the rotation angle (φ) of its molecules from 0º to 90º, the phase will be changed from -26º to -6º, respectively, as shown in Fig. 6 (b). Moreover, changing the positions of electrodes will vary the phase of the transmitted signal. Figures 6 (b) and 6 (c) show the numerical results of S_{21} for two different electrodes positions: along y-axis and along z-axis, respectively. It should be noted from these figures, that the position of electrodes along the z-axis results in phase shifter with wide tunable range from 6º to 83º for different biasing voltage at LC with thickness 4 mm, as shown in Fig. 7 (a).

Figures 7 (b) and 7 (c) show the steady state z-polarized magnetic field distributions along the *xy* plane at frequencies of 4 GHz and 4.53 GHz, respectively. It is evident from these figures that, the field along the structure is highly confined at port 1 at f = 4 GHz, while at f = 4.53 GHz the field propagates from port 1 to port 2. These field distributions confirm the behavior of S_{21} shown earlier in Fig. 6 (a). Figure 7 (d) demonstrates the steady state distributions of the *z*-polarized magnetic field along the propagation *x* direction at the wavelength of 9 mm for the chosen LC thicknesses δ = 4 mm with placing electrodes along *x*-axis at $\varphi = 0^o$ and $\varphi = 90^o$. It can be observed from the figure that, the transmitted signal at $\varphi = 90^o$ overrides the transmitted signal at $\varphi = 0^o$ by about $\ell = \lambda/4.5$, which clearly fits with the behavior of the argument of S_{21} shown in Figs. 6 (a) and 7 (a).

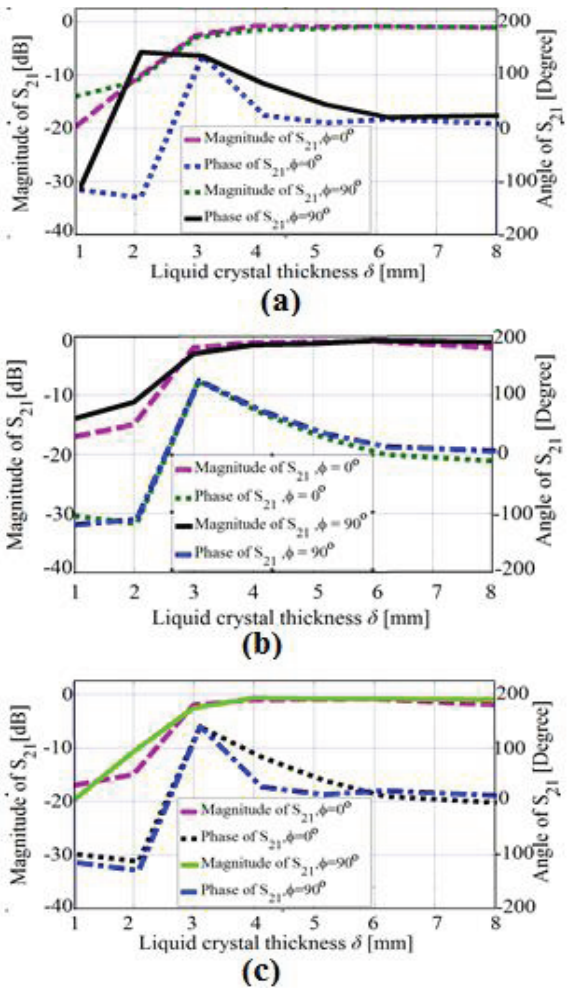

Fig. 6. Transmitted S-parameter vs. LC thickness at different electrode positions: (a) along x-axis, (b) along y-axis, and (c) along z-axis.

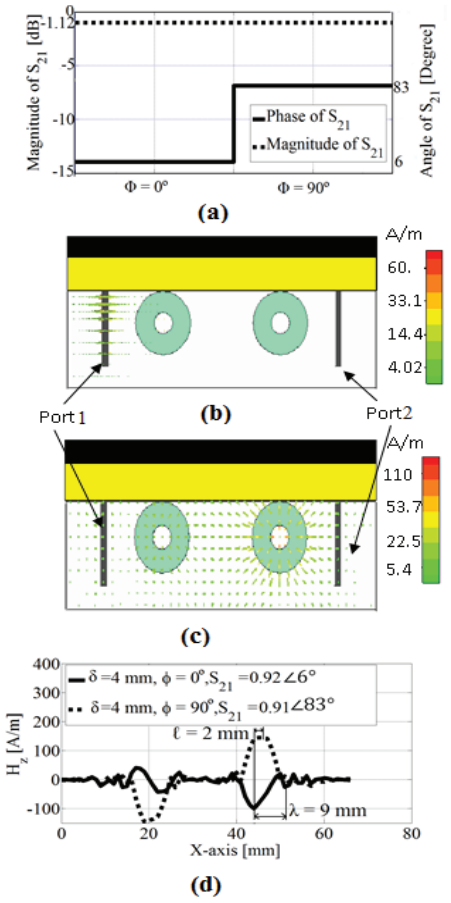

Fig. 7. (a) Electrical tunable phase shifter results for LC thickness of δ = 4 mm and the electrodes are positioned along *x*-axis, (b) 2D z-magnetic field along *xy*-plane at 4 GHz, (c) 2D z-magnetic field along *xy*-plane at 4.53 GHz, and (d) 1D z-magnetic field along *x-axis* at y = -10.3 mm and z = 8 mm.

It is evident from Fig. 8 that, the phase and magnitude of S_{21} will be decreased 66.5% and 2235%, respectively by increasing the wall thickness of the silica pan by around 50% from its original value (3 mm to 4.5 mm). However, the phase and magnitude of S_{21} will be decreased by 33.93% and 20.3%, respectively, by decreasing the silica pan wall thickness from 3 mm to 1.5 mm. This means that the performance of the suggested phase shifter is sensitive to the silica pan thickness. Figures 8 (c) and 8 (d) show the steady state z-polarized magnetic field distributions along the *xy*-plane at frequencies of 4 GHz and 4.53 GHz, respectively. It is evident from these figures that, the field along the structure is highly confined at port 1 at f = 4 GHz, while at f = 4.53 GHz the field propagates from port 1 to port 2. These field distributions are compatible with the behavior of S_{21} shown earlier in Figs. 8 (a) and 8 (b). Figure 8 (e) demonstrates the steady state distributions of the *z*-polarized magnetic field along the propagation *x* direction at the wavelength of 9 mm for the chosen silica pan wall thickness $\wp$ = 1.5 mm and $\wp$ = 4.5 mm, respectively with LC thicknesses δ = 4 mm. It can be observed from the figure that, the transmitted signal at $\wp$ = 4.5 mm overrides the transmitted signal at $\wp$ = 1.5 mm by about $\ell = \lambda/6$, which clearly fits with the behavior of the argument of S_{21} shown in Fig. 8 (b).

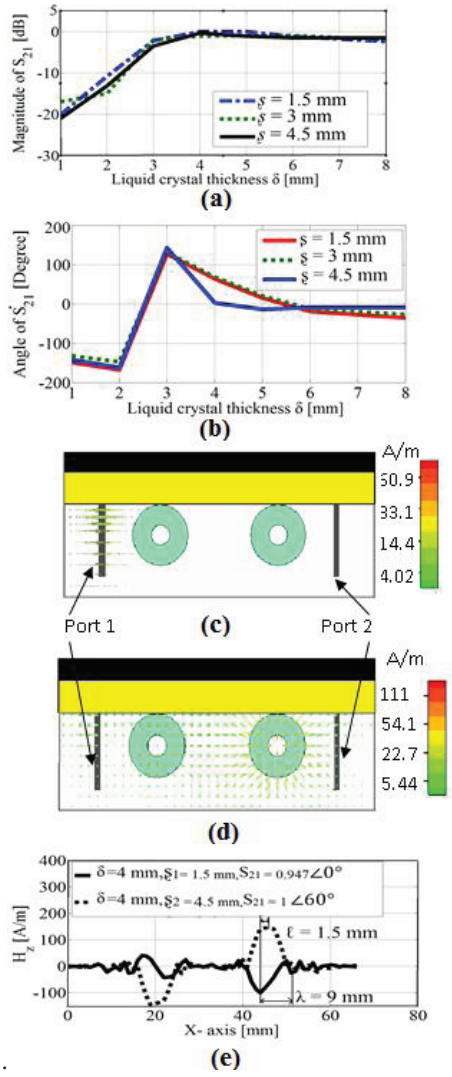

Fig. 8. Silica pan thickness variation at φ = 0º: (a) magnitude of S_{21}, (b) phase of S_{21}, (c) 2D z-magnetic field along *xy*-plane at 4 GHz, (d) 2D z-magnetic field along *xy*-plane at 4.53 GHz, and (e) 1D z-magnetic field along *x-axis* at y = -10.3 mm and z = 8 mm.

IV. CONCLUSION

The scope of this paper is to present a new simple design, highly compact and tunable phase shifter for different microwave applications. The proposed design is based for the first time to the best of our knowledge on the combination of dielectric resonators and nematic liquid crystal layer of type E7. Parametric study has been carried out to investigate the different geometrical parameters that affect the angle of S_{21}. Based on the simulation results, tunable phase shifter based on physical movement of the dielectric discs above the ground plane has been presented. However, the proposed novel design based on the use of NLC layers placed in silica pan as a substrate to the dielectric resonator overcomes the complexity of the phase shifter using physical movement. The suggested design has an excellent potential for being very useful in microwave encryption systems.

REFERENCES

[1] L. Zhou, Y. W. Yin, J. Wang, and S. L .Wu, "Dielectric resonators with high Q-factor for tunable low phase noise oscillators," *IEEE Trans. Components, Packaging and Manufacturing Tech.*, vol. 3, pp. 1008-1015, 2013.

[2] H. Hu and K.-L. Wu, "A TM_{11} dual-mode dielectric resonator filter with planar coupling configuration," *IEEE Trans. Microwave Theory Tech*., vol. 61, pp. 131-138, 2013.

[3] A. A. Kishk and W. Huang, "Size-reduction method for eielectric-resonator antennas," *IEEE Field, Waves, and Electromagnetics*, vol. 53, pp. 26-38, 2011.

[4] M. Memarian and R. Mansour, "Quad-Mode and Dual-Mode Dielectric Resonator Filters," *IEEE field, waves, and electromagnetics*, vol. 57, pp. 3418 - 3426, 2009.

[5] R. Saliminejad and M. R. Ghafourifard, "A novel and accurate method for designing dielectric resonator filter," *Progress In Electromagnetics Research B*, vol. 8, pp. 293-306, 2008.

[6] S. B. Cohn, "Microwave bandpass filters containing high-Q dielectric resonators," *IEEE Trans. Microwave Theory Tech*., vol. 16, pp. 218-227, 1968.

[7] S. J. Fiedziuszko, "Dual-mode dielectric resonator loaded DR cavity filters," *IEEE Trans. Microwave Theory Tech*., vol. 30, pp. 1311-1316, 1982.

[8] K. Wakino, T. Nishikawa, and Y. Ishikawa, "Miniaturization technologies of dielectric resonator filters for mobile communications," *IEEE Trans. Microwave Theory Tech*., vol. 42, pp. 1295-1300, 1994.

[9] R. R. Mansour, "Filter technologies for wireless base stations," *IEEE Microwave Magazine*, vol. 5, pp. 68-74, 2004.

[10] R. Vahidieck, "Design and development of high-Q microwave filters-past, present and future," *IEEE African*, vol. 2, pp. 1099-1104, 1999.

[11] C. Wang, H.-W. Yao, K. A. Zaki, and R. R. Mansour, "Mixed modes cylindrical planar dielectric resonator filters with rectangular enclosure," *IEEE Trans. Microwave Theory Tech*., vol. 43, pp. 2817-2823,1995.

[12] I. C. Hunter, J. D. Rhodes, and V. Dassonville, "Dual mode filters with conductor-loaded dielectric resonators," *IEEE Trans. Microwave Theory Tech*., vol. 47, pp. 2304-2311, 1999.

[13] G. Velu, K. Blary, L. Burgnies, A. Marteau, G. Houzet, D. Lippens, and J. Carru, "A 360° BST phase shifter with moderate bias voltage at 30 GHz," *IEEE Trans. Microwave Theory Tech*., vol. 55, no. 2, pp. 438-444, Feb. 2007.

[14] B. Pillans, S. Eshelman, A. Malczewski, J. Ehmke, and C. Goldsmith, "Ka-band RF MEMS phase shifters," *IEEE Microwave Guided Wave Letters*, vol. 9, pp. 520-522, 1999.

[15] R. Coats, J. Klein, S. Pritchett, and D. Zimmermann, "A low loss-monolithic five-bit pin diode phase shifter," *IEEE M1T-S International Microwave Symposium Digest*, vol. 2, pp. 915-918, 1990.

[16] M. F. O. Hameed and S. S. A. Obayya, "Highly nonlinear birefringent soft glass photonic crystal fiber with liquid crystal core," *IEEE Photonic Tech.*, vol. 23, pp. 1478-1480, 2011.

[17] http://www.cst.com/Content/Applications/Article/ArticlePDF.aspx?articleId=30.

[18] D Pinto and S. S. A. Obayya, "Improved complex-envelope alternating-direction-implicit finite-difference-time-domain method for photonic-bandgap cavities," *J. of Light Wave Tech*., vol. 25, no. 1, pp. 440-447, 2007.

[19] M Rajarajan, S. S. A. Obayya, B. M. A. Rahman, K. T. V. Grattan, and H. A. El-Mikali, "Characterization of low-loss waveguide bends with offset-optimisation for compact photonic

integrated circuits," *J. of Optoelectronics, IEE Proceedings*, vol. 147, no. 6, pp. 382-388, 2000.

[20]N Somasiri, B. M. A. Rahman, and S. S. A. Obayya, "Fabrication tolerance study of a compact passive polarization rotator," *J. of Light Wave Tech*., vol. 20, no. 4, pp. 751-757, 2002.

[21]N. Tucker, *Very Low Cost Electro-Mechanical Phase Shifter*, Technical Notes, 2010.

[22]N. F. F. Areed and S. S. A. Obayya, "Multiple image encryption system based on nematic liquid photonic crystal layers," *J. of Light Wave Tech*., vol. 32, no. 7, pp. 1344-1350, Jan. 2014.

[23]N. F. F. Areed and S. S. A. Obayya, "Novel all-optical liquid photonic crystal router," *J. of IEEE, Photonics Technology Letters*, vol. 25, no. 13, pp. 1254-1257, May 17, 2013.

[24]G. Ren, P. Shum, X. Yu, J. Hu, G. Wang, and Y. Gong, "Polarization dependent guiding in liquid crystal filled photonic crystal fibers," *Elsevier, Opt. Commun*., vol. 281, pp. 1598-1606, 2008.